nature synthesis

ARTICLES

https://doi.org/10.1038/s44160-022-00125-1

Check for updates

Brønsted acid-enhanced direct hydrogen atom transfer photocatalysis for selective functionalization of unactivated C(sp^3)–H bonds

Hui Cao[1,2], Degong Kong[1,3], Li-Cheng Yang[4,5,6], Supphachok Chanmungkalakul[7], Tao Liu[1], Jared L. Piper[8], Zhihui Peng[8], Linlin Gao[1], Xiaogang Liu[7], Xin Hong[4,5,6] ✉ and Jie Wu[1,2] ✉

The manipulation of unactivated aliphatic C–H bonds remains one of the most challenging tasks in synthetic chemistry. Direct hydrogen atom transfer (HAT) photocatalysis is an appealing approach to this goal. However, many methods are constrained due to low catalytic efficiency. Here we report the use of a Brønsted acid to enhance the efficiency of an inexpensive organic HAT photocatalyst, eosin Y. This strategy enables valuable transformations, including alkylation, heteroarylation and fluorination, of a wide array of unactivated C(sp^3)–H bonds, using the alkane substrate as the limiting reagent. The process has been applied to the late-stage functionalization of natural products and pharmaceuticals to selectively form C–H-functionalized analogues. Experimental and computational mechanistic studies show that the HAT reactivity is significantly enhanced when the sp^3 oxygen atoms on eosin Y are protonated. The method has been shown to be general across different types of direct HAT photocatalysts, demonstrating its potential in native C–H bond functionalization.

The catalytic functionalization of innate C(sp^3)–H bonds in organic molecules represents an ideal approach for molecule construction and editing[1,2]. Compared to activated $C(sp^3)$–H bonds adjacent to a heteroatom or π-system, the selective modification of unactivated C(sp^3)–H bonds presents a remarkable challenge due to their high bond dissociation energies (BDEs), low acidities and unreactive molecular orbital profiles[3]. In recent years, valuable technologies have been developed for the elaboration of unactivated C(sp^3)–H bonds via substrate-directed transition-metal C–H insertion[4], iridium-catalysed undirected borylation[5], rhodium-catalysed C–H insertion with donor–acceptor carbenoids[6], or HAT by electrophilic open-shell species[7–10]. Within this framework, direct HAT photocatalysis is an extremely appealing strategy due to the high catalyst and step economy (Fig. 1a)[11,12]. A direct HAT photocatalyst exploits the energy of a photon to trigger homolytic cleavage of the C(sp^3)–H bond with no need of any directing group or additive. The oxo group in the excited-state photocatalyst possesses O-centred radical character and could selectively abstract electron-rich and sterically accessible C(sp^3)–H bonds due to the polarity-matched HAT transition state[13]. The generated C-centred radical intermediates could be exploited for numerous C–C (refs. [14–17]), C–N (ref. [18]), C–O (ref. [19]), C–F (ref. [20]) and C–S (ref. [21]) bond formations. Although much progress has been achieved, the vast majority of established transformations require excess amounts of C–H substrates, especially for visible-light-absorbing photocatalysts[11,12]. The relatively low reactivity of direct HAT photocatalysts hampers their widespread application in the late-stage functionalization of advanced intermediates, pharmaceutical compounds and functional materials[22,23]. Notably, Britton and co-workers reported an accelerated C–H fluorination through an electrostatic interaction between ammonium-containing substrates and decatungstate catalyst[24]. However, apart from adjusting physical parameters (for example, light intensity) and using advanced engineering techniques (for example, flow technology)[17,18], a general strategy to enhance the reactivity of direct HAT photocatalysts remains unknown.

In this context, we took note of metal–oxygen complexes that could activate C(sp^3)–H bonds via proton-coupled electron transfer pathways, either stepwise or concerted[25]. With the elucidation of a Lewis acidic Ca^{2+} ion in the oxygen-evolving Mn_4CaO_5 cluster embedded in photosystem II, there has been increased interest in understanding the influence of Lewis or Brønsted acids binding to metal–oxygen complexes[26,27]. Fukuzumi, Nam and co-workers studied C(sp^3)–H oxidation reactions with $[(N4Py)Mn^{IV}(O)]^{2+}$ (**1**) and $[(N4Py)Mn^{IV}(O)]^{2+}$-$(HOTf)_2$ (**2**) (N4Py = *N*,*N*-bis(2-pyridylmethyl)-*N*-bis(2-pyridyl)methylamine, HOTf = triflic acid) (Fig. 1b)[28,29]. The binding of two HOTf molecules to the $Mn^{IV}(O)$ moiety results in a significant positive shift in the reduction potential. The oxidation of hexamethylbenzene (HMB) and pentamethylbenzene (PMB) by **2** proceeds via an electron transfer (ET) pathway at 273 K, and the observed reaction rate is much higher than that without HOTf. In the case of 1,4-cyclohexadiene (CHD), the highly endergonic ET reaction is unlikely at 298 K, and the HAT rate with **2** is actually decelerated by ~3-fold due to steric hindrance of the counter-anion of HOTf. An increase in ET reactivity and a decrease in HAT reactivity have also been observed when Lewis acids bind to metal–oxygen complexes[27,28]. Nevertheless, we questioned whether the binding of a Lewis or Brønsted acid to other heteroatoms adjacent to the oxo group could increase its electrophilicity without introducing steric hinderance. This strategy, if successful, would enhance the HAT reactivity of the oxo moiety.

[1]Department of Chemistry, National University of Singapore, Singapore, Republic of Singapore. [2]National University of Singapore (Suzhou) Research Institute, Suzhou, China. [3]School of Chemical Engineering & Technology, Harbin Institute of Technology, Harbin, China. [4]Center of Chemistry for Frontier Technologies, Department of Chemistry, State Key Laboratory of Clean Energy Utilization, Zhejiang University, Hangzhou, China. [5]Key Laboratory of Precise Synthesis of Functional Molecules of Zhejiang Province, School of Science, Westlake University, Hangzhou, China. [6]Beijing National Laboratory for Molecular Sciences, Beijing, China. [7]Singapore University of Technology and Design, Singapore, Republic of Singapore. [8]Chemical Research & Development, Worldwide Research Development & Medical, Pfizer Inc., Groton, MA, USA. ✉e-mail: hxchem@zju.edu.cn; chmjie@nus.edu.sg

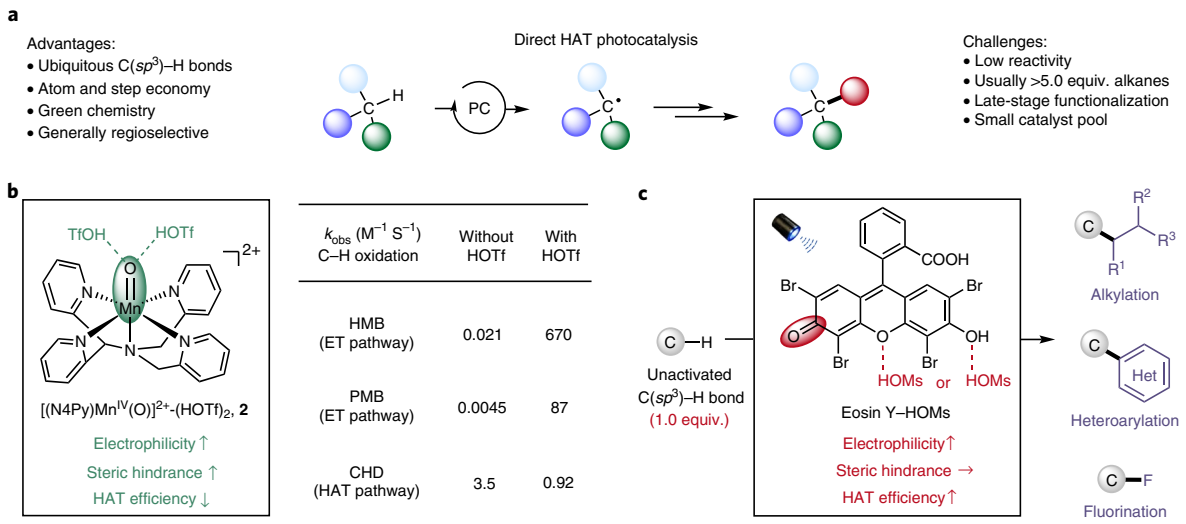

Fig. 1 | Development of a strategy to enhance the catalytic efficiency of direct HAT photocatalysis. a, The advantages and challenges of direct HAT photocatalysis[11,12]. **b**, Enhancing the ET reactivity of a metal-oxo complex with Brønsted acids[28,29]. **c** Enhancing the HAT reactivity of eosin Y with Brønsted acids (this work). PC, photocatalyst; ET, electron transfer; k, rate constant; HMB, hexamethylbenzene; PMB, pentamethylbenzene; CHD, 1,4-cyclohexadiene; HOM, methanesulfonic acid; Tf, triflyl; Ms, mesyl.

We recently reported that neutral eosin Y, an inexpensive organic dye, could behave as a visible-light-absorbing direct HAT photocatalyst for the functionalization of various activated C(sp^3)–H bonds[30–32]. The catalyst molecule can absorb a blue photon (~63 kcal mol^{-1}) to activate C–H bonds with BDEs of approximately 90 kcal mol^{-1}, beyond its redox capacity. However, low efficiencies were observed for unactivated C(sp^3)–H bonds (BDE > 96 kcal mol^{-1}), even when using five equivalents of alkane substrates. Compared to metal-oxo complexes, the eosin Y molecule possesses extra oxygen atoms on the xanthene core, offering opportunities to tune the HAT reactivity through interaction with acids (Fig. 1c).

Here we demonstrate the successful realization of this strategy for the eosin Y-photocatalysed functionalization of unactivated C(sp^3)–H bonds. Protonation by a common Brønsted acid, methanesulfonic acid, could significantly enhance the HAT reactivity of excited eosin Y, as evidenced by experimental and computational studies. Under blue light irradiation, regioselective C(sp^3)–H alkylation, heteroarylation and fluorination were achieved using alkanes as the limiting reagents. The late-stage functionalization of natural products and pharmaceutical molecules proceeded with good efficiency and high regioselectivity. Our preliminary results suggest that the protonation of heteroatoms near the oxo group could serve as a general strategy for enhancing the catalytic efficiency of direct HAT photocatalysts.

Results

Effects of acid additives in eosin Y photocatalysis. To explore the effect of acids on the HAT reactivity and site selectivity, 2,5-dimethylhexane (**3**), which contains three different types of unactivated C(sp^3)–H bonds, was selected as the standard alkane substrate and used as the limiting reagent. With electron-deficient alkene **4** as the reaction partner and 2 mol% neutral eosin Y as the direct HAT photocatalyst, the methine-functionalized product **5** was selectively obtained in 26% yield after 48 h under blue light irradiation (entry 1, Table 1). The product yield was barely improved by prolonged reaction time (entry 2). Subsequently, a series of acid additives were evaluated (Supplementary Tables 1 and 2). The addition of Lewis acids, however, resulted in even lower yields (entries 3–5). This can be explained by the selective binding of Lewis acids with the sp^2 oxygen atom in the carbonyl moiety[33], which increased the steric hindrance during the HAT process[27,28]. We reasoned that Brønsted acids could preferentially interact with more basic sp^3 oxygen atoms

Table 1 | Effect of acids on eosin Y-catalysed C(sp^3)–H alkylation

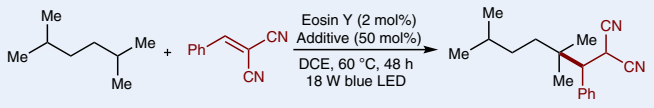

3 (1.0 equiv.) 4 (2.0 equiv.) 5

Entry[a]	Additive	Additive type	Yield (%)[b]	r.r.[c]
1	None	—	26	>20:1
2[d]	None	—	30	>20:1
3	$BF_3{\cdot}Et_2O$	Lewis acid	14	>20:1
4	$Yb(OTf)_3$	Lewis acid	15	>20:1
5	$Cu(OTf)_2$	Lewis acid	0	—
6	CF_3COOH	Brønsted acid	39	>20:1
7	CH_3SO_3H	Brønsted acid	81	>20:1
8	$pTSA{\cdot}H_2O$	Brønsted acid	47	>20:1
9	$HClO_4$	Brønsted acid	69	>20:1
10	Cs_2CO_3	Base	0	—

[a]Reaction conditions: **3** (0.2 mmol), **4** (0.4 mmol), neutral eosin Y (2 mol%) and additive (50 mol%) in DCE (4.0 ml) under irradiation using blue LEDs (470 nm) at 60 °C for 48 h under argon. [b]Yields were determined by analysis of the crude ^{1}H NMR spectra using dibromomethane as an internal standard. [c]Regioselectivity (r.r.) was determined by ^{1}H NMR spectroscopic and GC–MS analyses of the crude reaction mixture. [d]96 h reaction time. DCE, 1,2-dichloroethane; GC–MS, gas chromatography–mass spectrometry; LED, light-emitting diode; *p*TSA, *p*-toluenesulfonic acid.

(for example, protonated acetone pK_a −7.2 in H_2O (ref. [34]); protonated dimethyl ether pK_a −3.8 in H_2O (ref. [35])). To our delight, the efficiency of C(sp^3)–H alkylation was indeed increased by several Brønsted acids (entries 6–9), and the use of 50 mol% methanesulfonic acid delivered the most efficient transformation, affording the alkylated product **5** in good yield (81%) and regioselectivity (>20:1) (entry 7). In contrast, a base additive, caesium carbonate, completely inhibited the reaction (entry 10).

Mechanistic investigation on the acid effect. The dramatic enhancement of reaction efficiency prompted us to investigate the

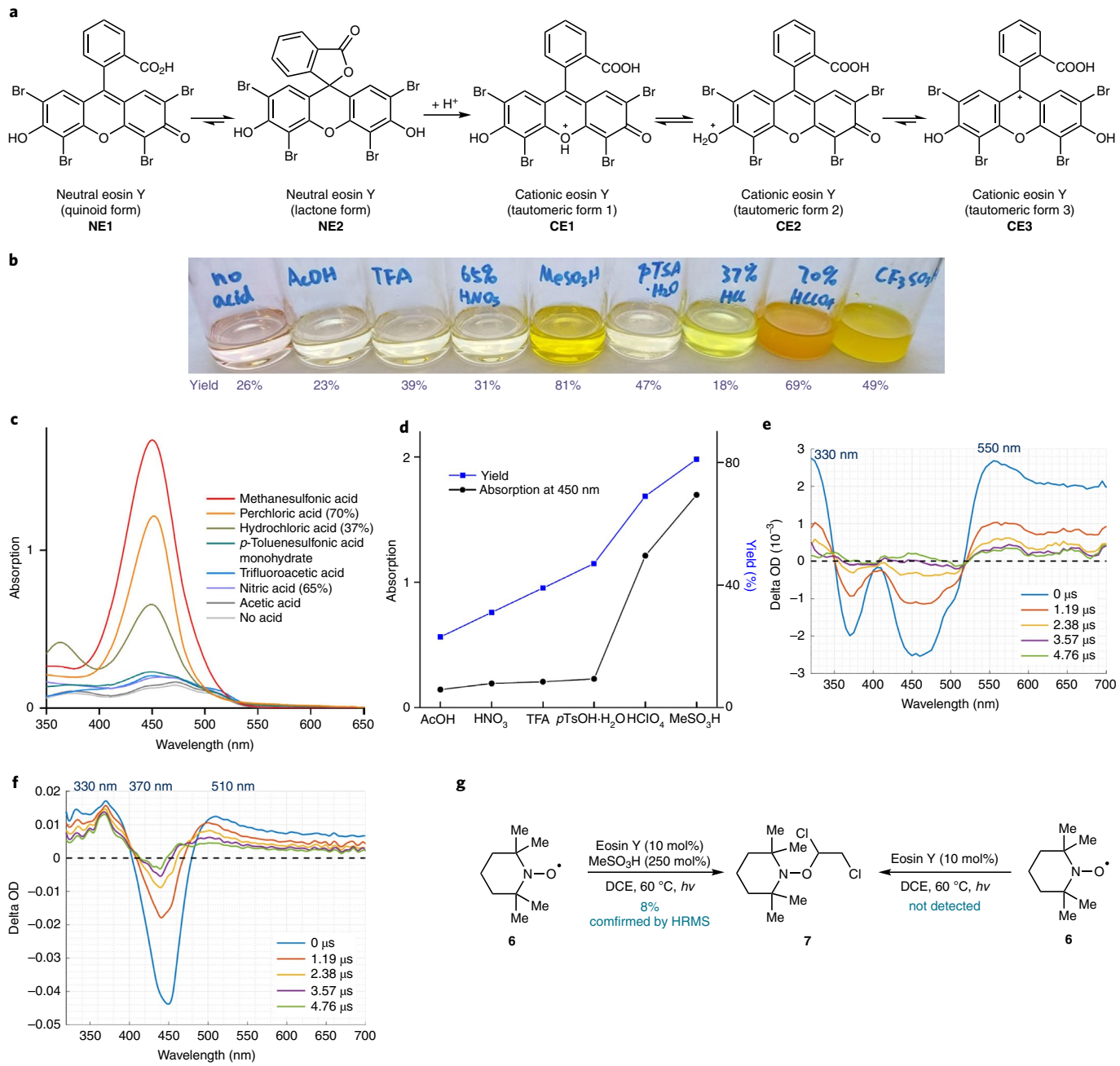

Fig. 2 | Mechanistic studies on the acid effect. a, Tautomeric forms of neutral eosin Y (**NE1** and **NE2**) and cationic eosin Y (**CE1**, **CE2** and **CE3**). **b**, Colour change after mixing neutral eosin Y (0.5 mM in DCE) with different Brønsted acids (12.5 mM, 25 equiv.). **c**, Ultraviolet–visible absorption spectra of eosin Y solutions (0.5 mM in DCE) mixed with different Brønsted acids (12.5 mM, 25 equiv.). No absorption spectrum was recorded for CF_3SO_3H because the mixture was opaque. **d**, Correlation between the absorption intensity at 450 nm (black) and the C(sp^3)–H alkylation yield (blue) with different Brønsted acids. **e**, Transient absorption spectrum of neutral eosin Y (0.2 mM) in DCE. **f**, Transient absorption spectrum of the mixture of neutral eosin Y (0.2 mM) and methanesulfonic acid (5 mM, 25 equiv.) in DCE. **g**, Trapping of the DCE radical with neutral eosin Y and cationic eosin Y. More details of mechanistic studies are included in the Supplementary Discussion. HRMS, high-resolution mass spectrometry; OD, optical density; TFA, trifluoroacetic acid.

role of Brønsted acids in eosin Y-mediated C(sp^3)–H functionalization. Eosin Y presents complex protolytic and tautomeric equilibria and could exist in different forms depending on the local pH and medium (Supplementary Fig. 4)[36,37]. The neutral species of eosin Y has two tautomeric forms: the quinoid form (**NE1**, Fig. 2a) and the spirocyclic lactone form (**NE2**). The quinoid form **NE1** has been proven by spectroscopic and computational studies to be HAT-active under blue light irradiation[30]. In the presence of Brønsted acids, the sp^3 oxygen atoms on eosin Y could be protonated to give three possible tautomeric forms of cationic eosin Y: **CE1**, **CE2** and **CE3** (Fig. 2a). Of these, **CE1** and **CE2** are potentially HAT-active under light irradiation considering their structural similarity to **NE1**. During the optimization of Brønsted acid additives, we observed that the light pink solution of neutral eosin Y quickly turned yellow after the addition of Brønsted acids (Fig. 2b). This was reflected by the change in the ultraviolet–visible absorption spectra (Fig. 2c). Neutral eosin Y showed relatively weak absorption in the visible-light region with maximum absorption at approximately

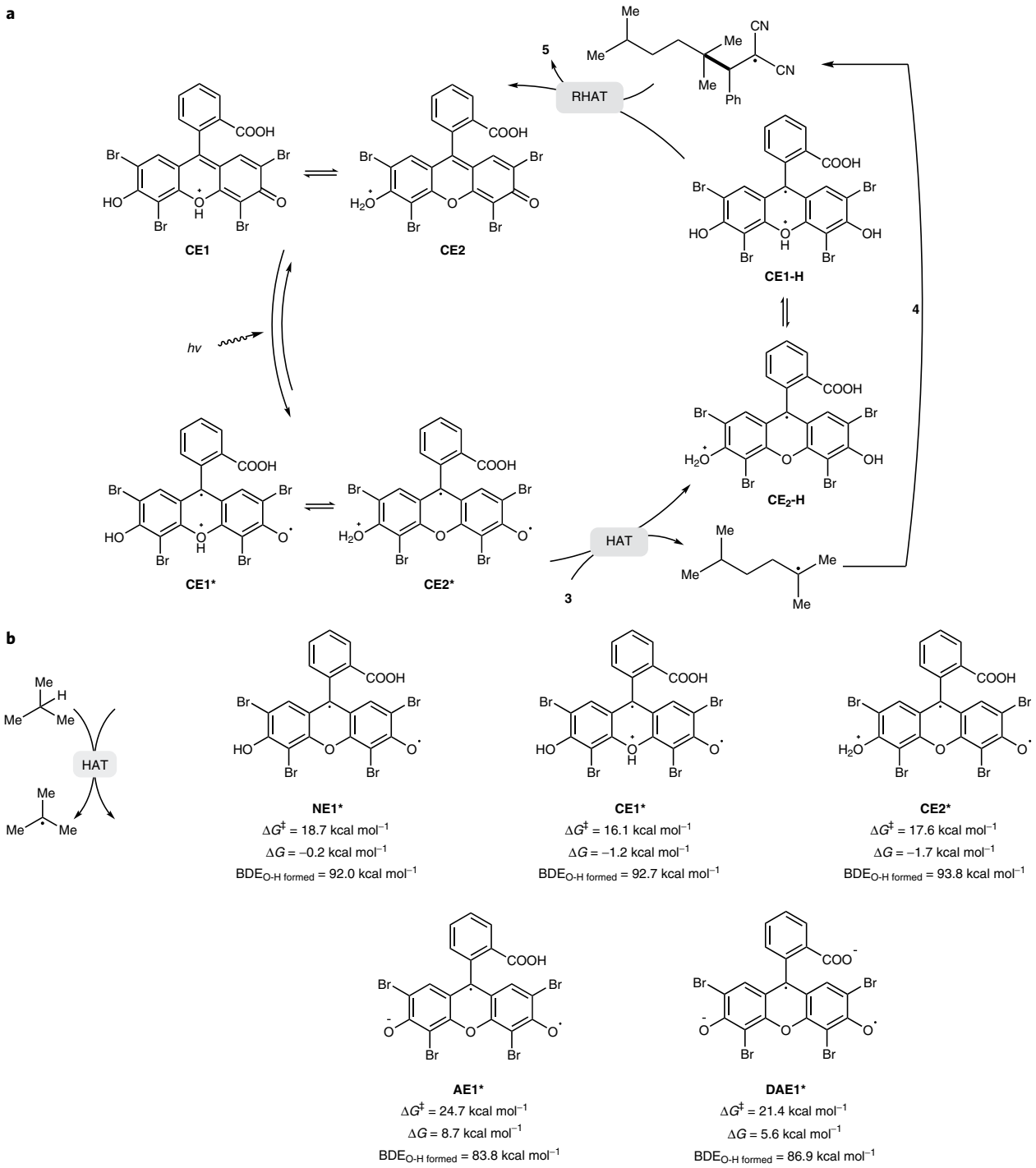

Fig. 3 | Proposed reaction mechanism and computational calculations on the HAT process. a, In the proposed mechanism, photoexcited cationic eosin Y (**CE1*** or **CE2***) abstracts a hydrogen atom from alkane **3**. The generated alkyl radical subsequently adds to alkene **4**. A reverse hydrogen atom transfer (RHAT) event between the radical adduct and cationic eosin Y-H (**CE1-H** or **CE2-H**) furnishes product **5** and regenerates the cationic eosin Y catalyst (**CE1** or **CE2**). **b**, DFT-computed free energy changes and formed O–H bond BDE values during HAT for different forms of eosin Y. Computational studies were performed at the ωB97X-D/def2-TZVP-SMD(DCE)//B3LYP-D3(BJ)/def2-SVP level of theory. More details are included in the Supplementary Discussion.

472 nm ($\varepsilon = 0.3 \times 10^3$ l mol^{-1} cm^{-1}), while a new strong absorption peak centred at approximately 450 nm ($\varepsilon = 3.5 \times 10^3$ l mol^{-1} cm^{-1}) appeared after methanesulfonic acid was added. In addition, the maximum emission peak of eosin Y shifted from 586 to 556 nm after the addition of acids (Supplementary Fig. 8), which indicated that the yellow species is a different species from neutral eosin Y. Mchedlov-Petrossyan observed that in water/sulfuric acid mixtures, neutral and cationic eosin Y showed absorption bands with peaks at approximately 480–485 nm ($\varepsilon = 8.5 \times 10^{-3}$ l mol^{-1} cm^{-1}) and 453-455 nm ($\varepsilon = 44.5 \times 10^{-3}$ l mol^{-1} cm^{-1}) at pH 0–0.5 and pH −2, respectively[38]. The reported equilibria and absorption data are consistent with our observations, suggesting that the new yellow species is protonated eosin Y (**CE1**–**CE3**). More importantly, it was noted that the Brønsted acids associated with stronger absorption

Table 2 | Substrate scope of C(sp^3)-H alkylation

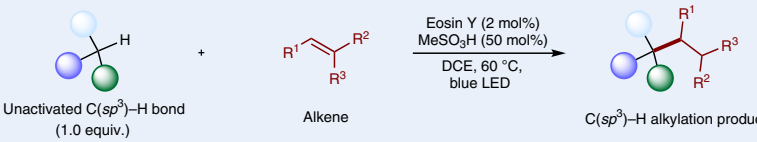

Unactivated C(sp^3)–H bond (1.0 equiv.) + Alkene → C(sp^3)–H alkylation product

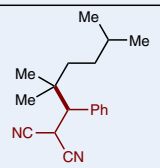

5, 88%, r.r. > 20:1 (29% without acid)

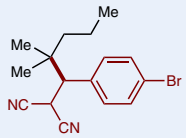

8, 74%, r.r. > 20:1

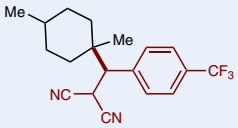

9, 72%[a], d.r. = 2:1

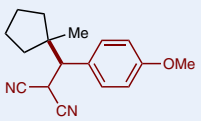

10, 62%, r.r. > 20:1

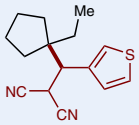

11, 59%[b]

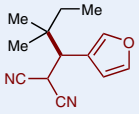

12, 37%, r.r. > 20:1

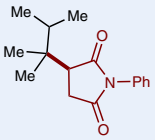

13, 82%, r.r. > 20:1 (24% without acid)

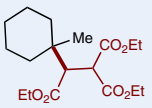

14, 75%[c]

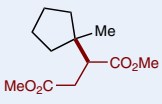

15, 70%, r.r. > 20:1 (18% without acid)

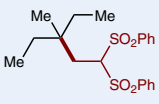

16, 71%, r.r. > 20:1 (25% without acid)

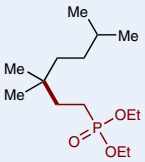

17, 51%, r.r. > 20:1

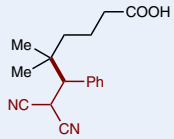

18, 82%, r.r. > 20:1 (20% without acid)

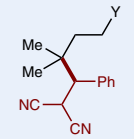

Y = Cl, **19**, 55%, r.r. > 20:1
Y = CN, **20**, 37%, r.r. > 20:1

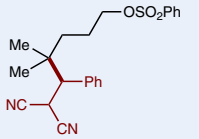

21, 73%, r.r. > 20:1

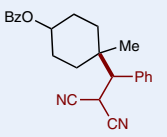

22, 66%, r.r. > 20:1
d.r. = 1.5:1

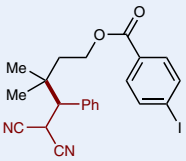

23, 44%, r.r. > 20:1

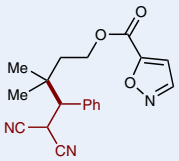

24, 76%, r.r. > 20:1

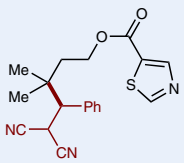

25, 40%, r.r. > 20:1

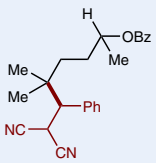

26, 72%, r.r. > 20:1
d.r. = 1.2:1

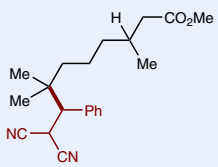

27, 93%, r.r. > 20:1
d.r. = 1:1

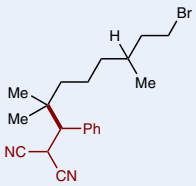

28, 50%, r.r. > 20:1
d.r. = 1:1

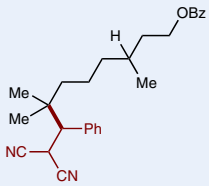

29, 85%, r.r. > 20:1
d.r. = 1:1

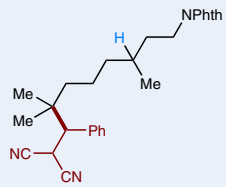

30, 69%, r.r. = 10:1[d], d.r. = 1:1

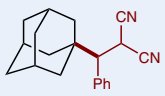

31, 45%, r.r. > 20:1

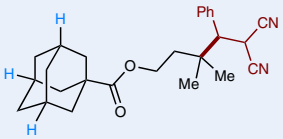

32, 55%, r.r. = 19:1[d]

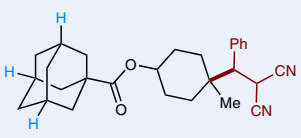

33, 40%, r.r. = 1:1[d], d.r. = 1.8:1

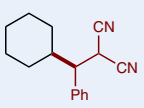

34, 53%
(12% without acid)

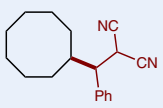

35, 78%

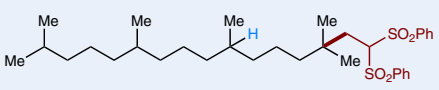

From pristane
36, 82%, r.r. = 1.3:1[d]

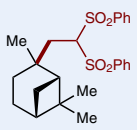

From pinane
37, 73%, r.r. > 20:1, d.r. > 20:1
71% (4 mmol scale, 1.26 g)

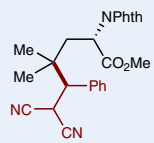

From leucine
38, 51%, r.r. > 20:1, d.r. = 1:1

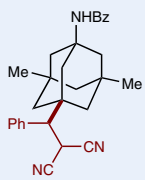

From memantine
39, 30%, r.r. > 20:1

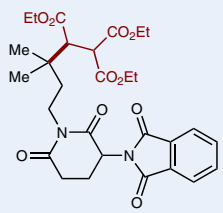

From thalidomide
40, 80%, r.r. > 20:1

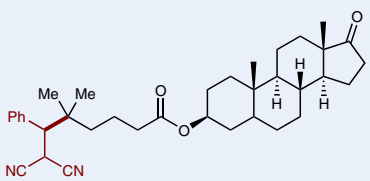

From androsterone
41, 39%, r.r. > 20:1

Reaction conditions: alkane (0.1 or 0.2 mmol, 1.0 equiv.), alkene (2.0 or 3.0 equiv.), neutral eosin Y (2 mol%) and methanesulfonic acid (50 mol%) in DCE (4 ml) under irradiation using a 40 W blue LED (λ_{max} = 467 nm) at 60 °C for 48–96 h under argon. Isolated yields are given. Regioselectivity (r.r.) and diastereomeric (d.r.) ratios were determined from ^{1}H NMR and GC–MS analyses of the crude reaction mixture. Bz, benzoyl; Phth, phthaloyl. [a]95% selectivity. [b]79% selectivity. [c]76% selectivity. [d]The minor activated C–H site is marked in blue.

Table 3 | Substrate scope of C(sp^3)–H heteroarylation

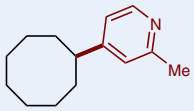

42, 74%
(44% without acid)

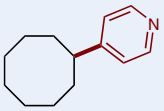

43, 89%

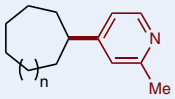

44, n = 1, 64%
45, n = 5, 65%

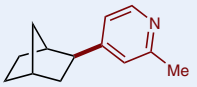

46, 38%, r.r. > 20:1
d.r. > 20:1

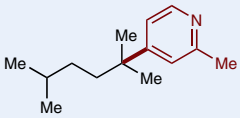

47, 15%[a], r.r. > 20:1

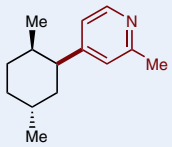

48, 56%, r.r. = 2.3:1[b]

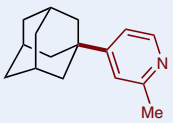

49, 84%, r.r. > 20:1
(47% without acid)

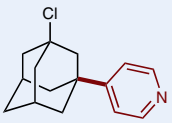

50, 86%, r.r. > 20:1

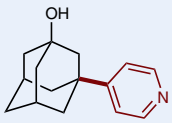

51, 72%, r.r. > 20:1

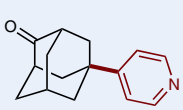

52, 45%, r.r. > 20:1
(19% without acid)

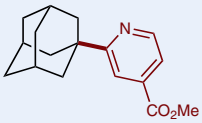

53, 37%, r.r. > 20:1

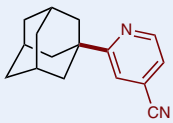

54, 34%, r.r. > 20:1

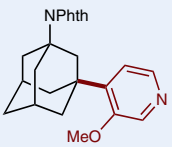

From amantadine
55, 65%, r.r. > 20:1

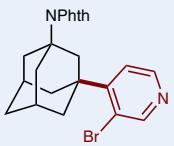

From amantadine
56, 83%, r.r. > 20:1

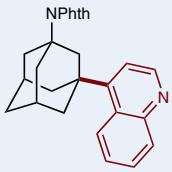

From amantadine
57, 39%, r.r. > 20:1

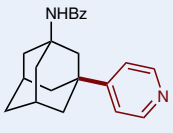

From amantadine
58, 78%, r.r. > 20:1

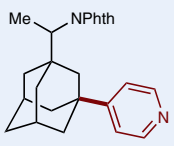

From rimantadine
59, 68%, r.r. > 20:1

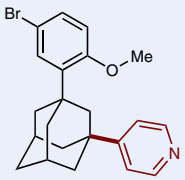

From adapalene precursor
60, 72%, r.r. > 20:1

Heteroarylation conditions: alkane (0.2 mmol, 1 equiv.), pyridinium salt (2 equiv.), neutral eosin Y (2 mol%) and methanesulfonic acid (50 mol%) in MeCN (4 ml) under irradiation using a 40 W blue LED (λ_{max} = 467 nm) at 60 °C for 48 h under argon. Isolated yields are given. Regioselectivity (r.r.) and diastereomeric (d.r.) ratios were determined from ^{1}H NMR spectroscopic and GC–MS analyses of the crude reaction mixture. [a]Yield determined by the analysis of crude ^{1}H NMR spectra using dibromomethane as an internal standard. [b]Minor regioisomer on methine position.

at 450 nm (intensified yellow colour) also led to higher reaction yields, except for volatile HCl (Fig. 2b,d). The most effective acid additive, methanesulfonic acid, gave rise to the strongest absorption at 450 nm. This strong correlation between absorption intensity and reaction efficiency indicated that protonated eosin Y is responsible for the enhanced reactivity.

A series of control experiments were carried out to further probe the catalytic process and elucidate the enhanced reactivity. First, fluorescence quenching experiments showed that neither alkane **3** nor alkene **4** could quench the excited state of cationic eosin Y (Supplementary Fig. 9). Various triplet photosensitizers failed to promote the C(sp^3)–H alkylation reaction (Supplementary Table 12). These observations suggest that an electron transfer or energy transfer pathway is unlikely and thereby support a HAT mechanism[30,39]. Next, a laser flash photolysis study was performed to identify the eosin Y transient intermediates. As shown in Fig. 2e, the DCE solution of neutral eosin Y exhibited a strong ground-state bleaching from 350 to 520 nm after laser excitation, and two new absorption peaks at approximately 330 and 550 nm decayed with very similar lifetimes (0.98 and 1.10 µs, respectively, Supplementary Fig. 11). These absorption peaks and lifetimes match the reported data of triplet-state neutral eosin Y (**NE1***, Fig. 3b)[30,39]. For the DCE solution of cationic eosin Y, strong bleaching of the ground state from 400 to 480 nm was observed upon laser excitation (Fig. 2f). In addition, two new absorption peaks at approximately 330 and 510 nm decayed with very similar lifetimes (3.74 and 4.18 µs, respectively, Supplementary Fig. 13). It should be noted that these two absorption peaks and decay lifetimes are different from those of the triplet state neutral eosin Y, indicating the presence of a different triplet state species. We assigned the absorption peaks at 330 and 510 nm to the excited cationic eosin Y (**CE1*** or **CE2***, Fig. 3b). Interestingly, another new absorption peak with an exceptionally long lifetime (323.7 µs, Supplementary Fig. 13) emerged at approximately 370 nm (Fig. 2f). This absorption and lifetime fit the characteristics of the radical intermediate neutral eosin Y-H, which could be generated by HAT from a hydrogen donor with excited neutral eosin Y (**NE1***)[30,39]. In stark contrast, the absorption peak at 370 nm corresponding to neutral eosin Y-H was not observed for neutral eosin Y in DCE (Fig. 2e)[39]. This comparison suggests that excited cationic eosin Y possesses stronger hydrogen-abstracting ability and could abstract a hydrogen atom from the relatively electron-poor and strong C–H bond in DCE ($BDE_{C-H} \approx 97$ kcal mol^{-1})[40]. Radical trapping experiments with TEMPO (**6**, (2,2,6,6-tetramethylpiperidin-1-yl)oxyl) further proved that excited cationic eosin Y could activate the C–H bonds in DCE, whereas excited neutral eosin Y could not (Fig. 2g). The presence of protonated eosin Y throughout the reaction process was supported by ultraviolet–visible monitoring (Supplementary Figs. 25 and 26) and electrospray ionization mass spectrometry (ESI-MS, Supplementary Figs. 27–29). Both light on/off experiments (Supplementary Fig. 30) and the calculated quantum yield (Φ = 0.004) supported a photocatalytic cycle with short-lived radical chain propagation[41]. A deuterium labelling study was also conducted by treating cyclohexane and d_{12}-cyclohexane with alkene **4** in two different vessels or in one vessel, resulting in k_H/k_D values of 2.5 and 3.5, respectively (Supplementary Fig. 24). The kinetic isotope effect (KIE) data indicated that C–H cleavage

Table 4 | Substrate scope of C(sp^3)–H fluorination

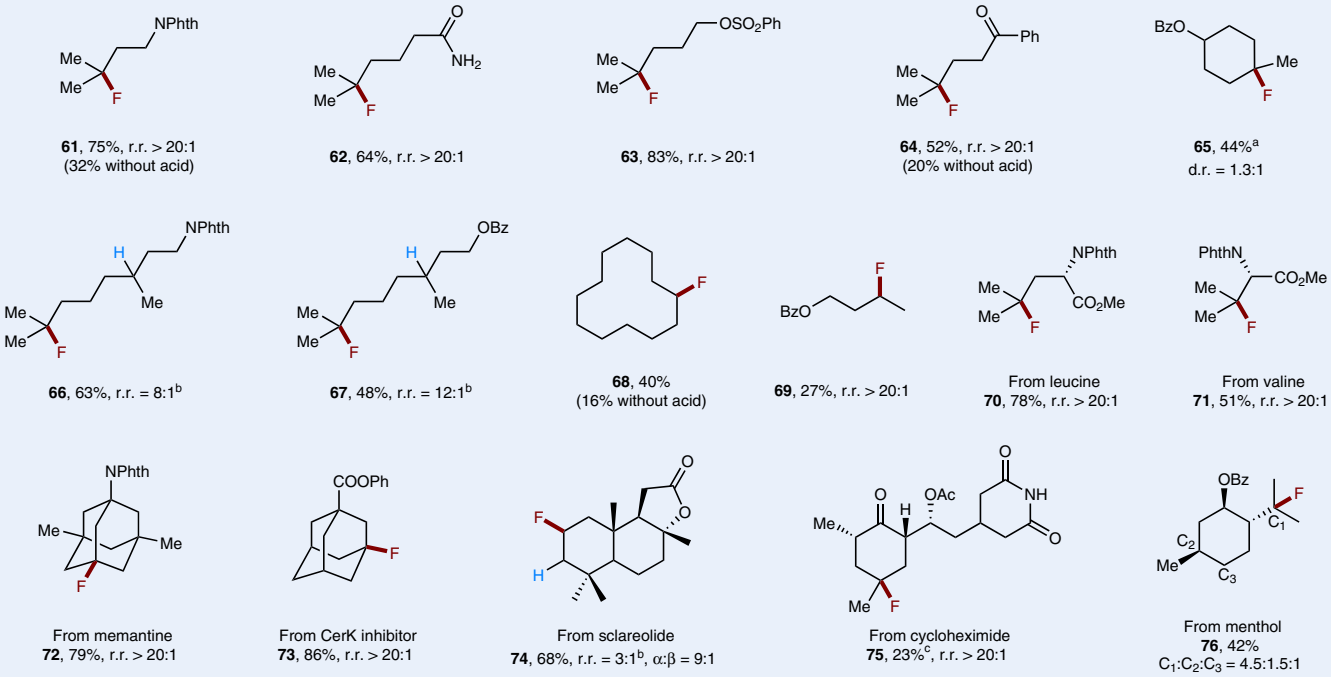

Fluorination conditions: alkane (0.2 mmol, 1 equiv.), Selectfluor (2 equiv.), neutral eosin Y (4 mol%) and methanesulfonic acid (100 mol%) in $MeCN/H_2O$ (1.5 ml/2.5 ml) under irradiation using a 40 W blue LED (λ_{max} = 467 nm) at 45 °C for 3 h under argon; then another portion of neutral eosin Y (4 mol%) was added and continuously irradiated for another 3 h. Isolated yields are given. Regioselectivity (r.r.) and diastereomeric (d.r.) ratios were determined from ^{1}H NMR spectroscopic and GC–MS analyses of the crude reaction mixture. [a]64% selectivity. [b]The minor activated C–H site is marked in blue. [c]Yield determined by the analysis of crude ^{1}H NMR spectra using dibromomethane as an internal standard.

might be involved in the rate-determining step[42]. A photo HAT cycle catalysed by protonated eosin Y was proposed in light of all the experimental data (Fig. 3a).

Our subsequent efforts were directed toward understanding the HAT reactivity difference through density functional theory (DFT) calculations (Fig. 3b). For the triplet cationic eosin Y **CE1*** and **CE2***, the computed free energy barriers of the HAT reaction with isobutane are 16.1 and 17.6 kcal mol^{-1}, respectively. Both are lower than the 18.7 kcal mol^{-1} HAT barrier of triplet neutral eosin Y (**NE1***). In addition, the barriers for triplet monoanionic (**AE1***) and dianionic (**DAE1***) eosin Y are above 21 kcal mol^{-1}, which is consistent with the poor HAT performance in the presence of a base (entry 10, Table 1). The kinetic trend agrees well with the thermodynamic driving force. For protonated eosin Y, the calculated BDEs of the O–H bonds formed during HAT are also higher than those of neutral eosin Y (Fig. 3b), while anionic eosin Y possesses much weaker O–H bonds (see Supplementary Fig. 40 for the details of BDE calculation). Overall, these calculation results support the enhanced hydrogen abstraction power of triplet cationic eosin Y, which is most probably the reason for the improved catalytic efficiency.

Scope of C(sp^3)–H functionalizations. Having gained insight into Brønsted acid-enhanced direct HAT photocatalysis using eosin Y, we explored the scope and site selectivity of this C–H alkylation process (Table 2). A wide range of unactivated alkanes were smoothly alkylated in moderate to excellent yields with the C–H substrate as the limiting reagent (**5** and **8**–**41**). Hydrocarbons, including cyclic and acyclic ones, gave alkylated products **5** and **8**–**17** in good yields (37–88%) with high selectivity on the most electron-rich methine sites. Steric hindrance had little effect on the alkylation reactivity, and even 2,3-dimethylbutane gave product **13** in 82% yield. The regioselectivity was decreased to some extent when the substrates possessed more methylene C–H bonds (**11** and **14**). A series of aryl groups on methylenemalononitrile were tolerated, bearing functional groups such as aryl bromide (**8**), trifluoromethyl (**9**), thiophene (**11**) and furan (**12**). Michael acceptors possessing amide (**13**), ester (**14**, **15**), sulfone (**16**) or phosphate ester (**17**) moieties were all good candidates for this transformation, affording the corresponding products in 51–82% yields. Control experiments consistently showed that the reaction yield was significantly improved in the presence of methanesulfonic acid (**5**, **13**, **15**, **16**, **18** and **34**). Functional alkanes with terminal electron-withdrawing groups were subsequently evaluated (**18**–**30**). Different functional groups, such as free carboxylic acid (**18**), alkyl chloride (**19**), nitrile (**20**), benzenesulfonate (**21**), aryl iodide (**23**), isoxazole (**24**), thiazole (**25**) and alkyl bromide (**28**), were well tolerated. C–H bond alkylation was found to be highly selective for reactions at more electron-rich, remote, methine C–H bonds (**18**–**25**). In addition, excellent regioselectivity was observed for remote methine C–H bonds over proximal ones (**26**–**30**), revealing the inherent electronic selectivity of the HAT process[13]. A 45% yield of methine-functionalized product was obtained with adamantane (**31**). The transformation of adamantane derivatives showed that the methine C–H bonds were preferentially functionalized in the presence of an adamantane group (**32** and **33**), presumably

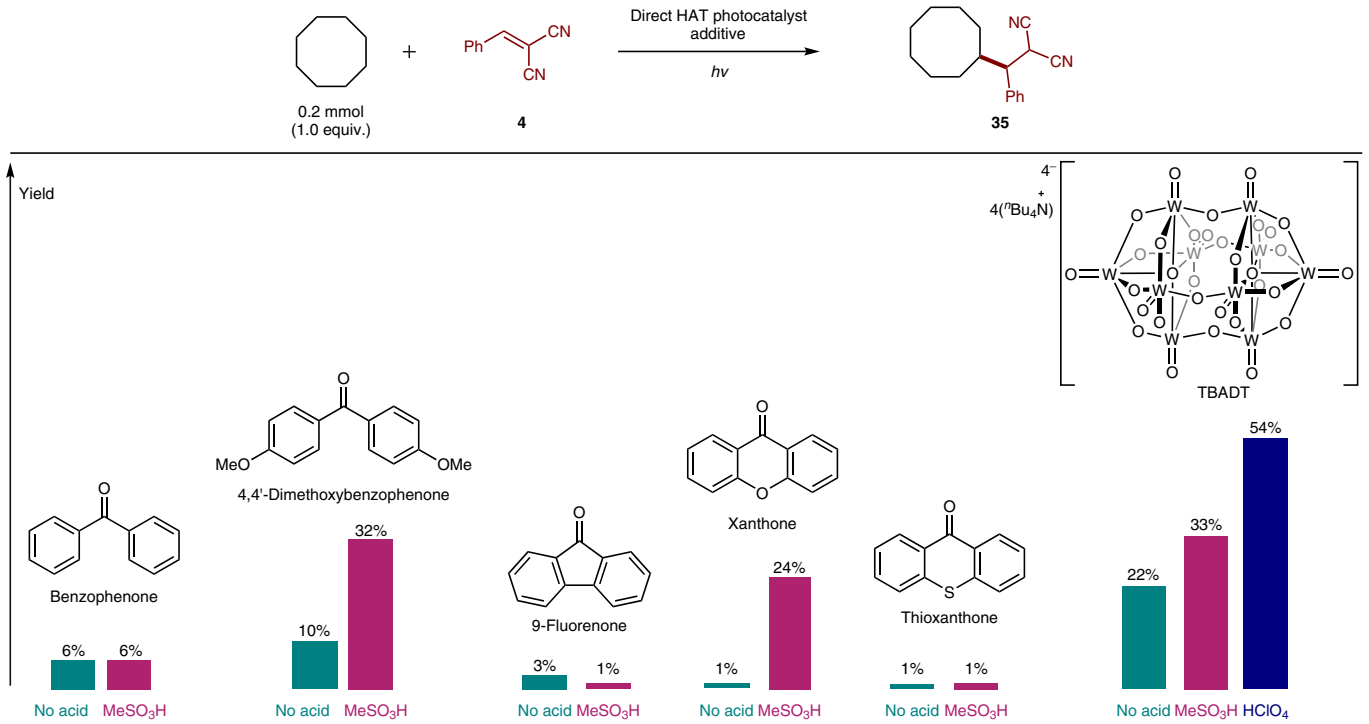

Fig. 4 | Effect of Brønsted acids on different direct HAT photocatalysts. Enhancement of HAT efficiency with Brønsted acid was observed for aromatic ketones bearing sp^3 oxygen atoms and the decatungstate anion. Reaction conditions for aromatic ketones: cyclooctane (0.2 mmol, 1.0 equiv.), alkene **4** (2.0 equiv.), ketone photocatalyst (50 mol%) and acid (25 mol%, if used) in DCE (2 ml) under irradiation using 40 W LED (λ_{max} = 390 nm) at 60 °C for 24 h under argon. Reaction conditions for TBADT: cyclooctane (0.2 mmol, 1.0 equiv.), alkene **4** (1.0 equiv.), TBADT (1 mol%) and acid (20 mol%, if used) in MeCN (2 ml) under irradiation using 40 W LED (λ_{max} = 370 nm) at room temperature for 2 h under argon. Yields were determined by analysis of the crude ^{1}H NMR spectra using dibromomethane as an internal standard.

due to electronic effects and the relatively high BDE of adamantane methine C–H bonds (~99 kcal mol^{-1})[40]. The unactivated methylene C–H bonds in cyclic alkanes were readily accommodated (**34** and **35**). The potential of this protocol for the late-stage site-selective alkylation of complex molecules was subsequently investigated. Pristane, a natural saturated terpenoid, was alkylated in excellent yield (82%) with a slight preference for the more sterically accessible terminal methine sites (**36**). A mixture of diastereomers of pinane containing three electronically similar but sterically distinct methine C–H bonds reacted to give 73% isolated yield of a single isomer **37**. Scaling up the alkylation reaction to 4 mmol delivered 1.26 g of **37** with similar efficiency. Useful yields were observed for the essential amino acid leucine (**38**) and the drug memantine (**39**) with exclusive regioselectivity at the methine sites. Similarly, the complex derivatives of thalidomide (**40**) and androsterone (**41**) underwent regiospecific alkylation in 80% and 39% yields, respectively.

The efficient and site-selective activation of alkanes by Brønsted acid-enhanced direct HAT photocatalysis sets the stage for installing medicinally relevant functionalities in molecular scaffolds. We found that this strategy can be readily applied to C(sp^3)–H heteroarylation and fluorination using C–H substrate as the limiting reagent (Tables 3 and 4). The use of methanesulfonic acid was crucial for an efficient transformation in both transformations (**42**, **49**, **52**, **61**, **64**, **68**). With *N*-aminopyridinium salt as the reaction partner[43], cyclic alkanes with ring sizes ranging from 7 to 12 gave the 4-pyridinated products **42**–**45** in good yields (64–89%). The methylene C–H bonds in norbornane (**46**) reacted selectively in the presence of sterically hindered methine C–H bonds. Interestingly, 2,5-dimethylhexane, which was a good candidate in the alkylation reaction (88% yield, **7**), afforded the pyridination product in poor yield (15%, **47**). Moreover, *trans*-1,4-dimethylcyclohexane, which exhibited high methine selectivity in alkylation (**9**, r.r. = 19:1), underwent selective pyridination on the methylene sites (**48**, r.r. = 2.3:1). The inverse reactivity and selectivity could be rationalized by the relatively slow addition of bulky tertiary alkyl radicals to heteroarenes[44]. Compared to Giese-type reactions, the Minisci-type reaction is more sensitive to steric hindrance around the radical centre[45]. Adamantane-containing compounds were then examined because of their unique physicochemical and biological properties. The reaction of adamantane derivatives, including amantadine (**55**-**58**), rimantadine (**59**) and an adapalene precursor (**60**), furnished the heteroaryl products in generally good yields (39–83%). Pyridination occurred predominantly at the methine C–H sites, presumably due to their equatorial character and the high stability of 1-adamantyl radicals[46,47]. Electron-poor and electron-rich substituents at either the C2 (**49**) or C3 (**55**, **56**) position of pyridine had little influence on the reaction efficiency. C4-substituted pyridinium salts could also be accommodated, delivering 2-pyridinated products in moderate yields (**53**, **54**). In addition, a quinolinium salt was an effective substrate to afford **57**. We next explored the direct fluorination of unactivated C(sp^3)–H bonds in view of the critical role fluorine plays in drug development[48]. With Selectfluor (1-chloromethyl-4-fluoro-1,4-diazoniabicyclo[2.2.2]octane bis(tetrafluoroborate)) as the fluorination reagent, fluorine substitution occurred with a broad range of substrates with generally good efficiency and high selectivity (**61**–**76**). C–H fluorination occurred selectively at the more electron-rich methine C–H bonds (**61**–**67**), tolerating functional groups such as protected amine (**61**), amide (**62**) and ketone (**64**). Cyclododecane afforded the monofluorinated product **68** in 40% yield. Interestingly, the remote methylene C–H bonds in butyl benzoate (**69**) were selectively functionalized (r.r. > 20:1). We were pleased to observe that a number of natural products and pharmaceuticals participated in efficient fluorination with our protocol (**70**–**76**). Fluorinated amino acids are valuable intermediates in drug

discovery and potential imaging agents for cancer[49]. We managed to obtain a 78% yield of γ-fluorinated leucine (**70**), which serves as a precursor to the investigational drug odanacatib. Another amino acid, valine, was also an effective substrate (**71**, 51%). Two adamantane-containing drugs (**72** and **73**) were selectively fluorinated in excellent yields (79% and 86%, respectively). Difluoro and trifluoro products, which are observed in electrochemical C–H fluorination, were not detected in any of these reactions[50]. Sclareolide, a sesquiterpenoid natural product, was fluorinated at sterically accessible methylene sites (**74**, 68%). The naturally occurring fungicide cycloheximide, which contains five methine C–H bonds and five methylene sites, underwent fluorination exclusively on the most hydridic methine C–H bond, albeit in lower yield (**75**). Menthyl benzoate with two electronically similar methine C–H bonds reacted preferentially at the isopropyl side chain (**76**, 64% selectivity for C1). Notably, this selectivity is different from that of decatungstate-photocatalysed fluorination[20] and iron-catalysed oxidation[51], where functionalization of the less-hindered cyclohexyl methine site (C2) is preferred. The observed selectivity in our reaction indicates that photoexcited protonated eosin Y is less sensitive to steric hindrance, which is consistent with our design principle (Fig. 1).

Effect of acid on other direct HAT photocatalysts. We further investigated whether this strategy could be a general method to enhance the reactivity of direct HAT photocatalysis. Considering the widespread usage of aromatic ketones and decatungstate anion in photocatalysed HAT reactions[11,12], the effect of Brønsted acids on these ultraviolet-light-absorbing photocatalysts was investigated. As shown by the preliminary results (Fig. 4), no improvement in HAT efficiency was observed for benzophenone with the addition of methanesulfonic acid. However, for 4,4′-dimethoxybenzophenone bearing sp^3 oxygen atoms, the alkylation yield was increased from 10% to 32% in the presence of the same acid. Moreover, a 24-fold increase in reaction yield was obtained for xanthone, presumably owing to the proximity of its sp^3 oxygen atom to the carbonyl moiety. In contrast, 9-fluorenone and thioxanthone, two structural analogues of xanthone that lack sp^3 oxygen atoms, showed no improvement in product yield in the presence of an acid. These results suggest that the protonation of sp^3 oxygen atoms in an aromatic ketone photocatalyst could lead to enhanced HAT efficiency. The alkylation yield with tetra-n-butylammonium decatungstate (TBADT) was also improved (from 22% to 33% yield) by the use of methanesulfonic acid. A stronger Brønsted acid, perchloric acid, further improved the reaction yield to 54%. The improvement was most likely due to protonation of the sp^3 oxygen atoms in the W–O–W bonds of TBADT[52].

Discussion

We report here a general strategy for enhancing the reactivity of direct HAT photocatalysts with Brønsted acids. With eosin Y as an economic choice for HAT photocatalysts, this approach provides a general platform for the functionalization of unactivated alkanes using C–H substrate as the limiting reagent. Late-stage functionalizations, including alkylation, heteroarylation and fluorination, of complex pharmaceutically important molecules were achieved with high levels of site selectivity, and a broad scope of functional groups were tolerated. The selective protonation of sp^3 oxygen atoms on eosin Y results in significantly enhanced HAT efficiency, as evidenced by experimental and computational findings. Brønsted acid-enhanced HAT was also found to be applicable to aromatic ketones and decatungstate anions. This study is expected to inspire further efforts at C–H functionalization via HAT catalytic pathways.

Methods

General procedure for C(sp^3)–H alkylation. To a 10 ml oven-dried Schlenk tube equipped with a magnetic stir bar, the corresponding C–H nucleophile (0.1 or 0.2 mmol, 1.0 equiv., if solid), alkene (2 or 3 equiv.), eosin Y (2 mol%) and DCE (4 ml) were added. The resulting mixture was cooled to 0 °C using an ice-water bath and bubbled with an argon balloon for 10 min. Methanesulfonic acid (50 mol%) and the C–H nucleophile (0.1 or 0.2 mmol, 1.0 equiv., if liquid) were then added. After that, the reactor was placed close to a 40 W 467 nm LED (~3 cm away), stirred and irradiated for 48 or 96 h under argon atmosphere. The temperature was maintained at 60 °C using a water bath. The reaction mixture was removed from the light and quenched by stirring while open to air for 5 min. The solvent was removed on a rotary evaporator under reduced pressure, and the residue was subjected to column chromatography isolation over silica gel or preparative thin-layer chromatography to give the corresponding product.

General procedure for C(sp^3)–H heteroarylation. To a 10 ml oven-dried Schlenk tube equipped with a magnetic stir bar, the corresponding C–H nucleophile (0.2 mmol, 1.0 equiv., if solid), pyridinium salt (0.4 mmol, 2 equiv.), eosin Y (2.6 mg, 0.004 mmol, 2 mol%) and acetonitrile (4 ml) were added. The resulting mixture was cooled to 0 °C using an ice-water bath and bubbled with an argon balloon for 10 min, followed by the addition of methanesulfonic acid (9.6 mg, 0.1 mmol, 50 mol%) and the C–H nucleophile (0.2 mmol, 1.0 equiv., if liquid). After that, the reactor was placed close to a 40 W 467 nm LED (~3 cm away), stirred and irradiated for 48 h under argon atmosphere. The temperature was maintained at 60 °C using a water bath. The reaction mixture was removed from light and quenched by stirring while open to air for 5 min. The solvent was removed on a rotary evaporator under reduced pressure. Then, 5 ml of saturated $NaHCO_3$ aqueous solution was added, and the reaction mixture was extracted by dichloromethane (3 × 5 ml). The combined organic phase was dried over $MgSO_4$ and concentrated under reduced pressure. Column chromatography isolation over silica gel or preparative thin-layer chromatography gave the corresponding product.

General procedure for C(sp^3)–H fluorination. To a 10 ml oven-dried Schlenk tube equipped with a magnetic stir bar, the corresponding C–H nucleophile (0.2 mmol, 1.0 equiv., if solid), Selectfluor (141.7 mg, 0.4 mmol, 2 equiv.), eosin Y (5.2 mg, 0.008 mmol, 4 mol%), water (2.5 ml) and acetonitrile (1.5 ml) were added. The resulting mixture was cooled to 0 °C using an ice-water bath and bubbled with an argon balloon for 10 min. Methanesulfonic acid (19.2 mg, 0.2 mmol, 100 mol%) and the C–H nucleophile (0.2 mmol, 1.0 equiv., if liquid) were then added. Next, the reactor was placed close to a 40 W 467 nm LED (~3 cm away), stirred and irradiated for 3 h under argon atmosphere. The temperature was maintained at 45 °C using a water bath and cooling fan. Another portion of eosin Y (5.2 mg, 0.008 mmol, 4 mol%) was added under an argon atmosphere, and the reaction was again subjected to light irradiation for 3 h. The reaction was removed from light and quenched by stirring while open to air for 5 min. The mixture was diluted with water and extracted with dichloromethane (3 × 5 ml). The combined organic phase was dried over $MgSO_4$ and concentrated under reduced pressure. Column chromatography isolation over silica gel or preparative thin-layer chromatography gave the corresponding product.

Data availability

All data supporting the findings of this study are available within the paper and its Supplementary Information. The Cartesian coordinates of the calculated stationary points are provided in the Supplementary Data.

Received: 26 January 2022; Accepted: 23 June 2022;
Published online: 04 August 2022

References

1. Davies, H. M. L., Du Bois, J. & Yu, J.-Q. C–H functionalization in organic synthesis. *Chem. Soc. Rev.* **40**, 1855–1856 (2011).
2. Wencel-Delord, J. & Glorius, F. C–H bond activation enables the rapid construction and late-stage diversification of functional molecules. *Nat. Chem.* **5**, 369–375 (2013).
3. Xue, X. S., Ji, P., Zhou, B. & Cheng, J. P. The essential role of bond energetics in C–H activation/functionalization. *Chem. Rev.* **117**, 8622–8648 (2017).
4. Sambiagio, C. et al. A comprehensive overview of directing groups applied in metal-catalysed C–H functionalisation chemistry. *Chem. Soc. Rev.* **47**, 6603–6743 (2018).
5. Oeschger, R. et al. Diverse functionalization of strong alkyl C–H bonds by undirected borylation. *Science* **368**, 736–741 (2020). (2020).
6. Liao, K., Negretti, S., Musaev, D. G., Bacsa, J. & Davies, H. M. L. Site-selective and stereoselective functionalization of unactivated C–H bonds. *Nature* **533**, 230–234 (2016).
7. Hu, A., Guo, J.-J., Pan, H. & Zuo, Z. Selective functionalization of methane, ethane, and higher alkanes by cerium photocatalysis. *Science* **361**, 668–672 (2018).
8. An, Q. et al. Cerium-catalyzed C–H functionalizations of alkanes utilizing alcohols as hydrogen atom transfer agents. *J. Am. Chem. Soc.* **142**, 6216–6226 (2020).
9. Shu, C., Noble, A. & Aggarwal, V. K. Metal-free photoinduced C(sp^3)–H borylation of alkanes. *Nature* **586**, 714–719 (2020).

10. Fazekas, T. J. et al. Diversification of aliphatic C–H bonds in small molecules and polyolefins through radical chain transfer. *Science* **375**, 545–550 (2022).
11. Cao, H., Tang, X., Tang, H., Yuan, Y. & Wu, J. Photoinduced intermolecular hydrogen atom transfer reactions in organic synthesis. *Chem. Cat.* **1**, 523–598 (2021).
12. Capaldo, L., Ravelli, D. & Fagnoni, M. Direct photocatalyzed hydrogen atom transfer (HAT) for aliphatic C–H bonds elaboration. *Chem. Rev.* **122**, 1875–1924 (2022).
13. Ravelli, D., Fagnoni, M., Fukuyama, T., Nishikawa, T. & Ryu, I. Site-selective C–H functionalization by decatungstate anion photocatalysis: synergistic control by polar and steric effects expands the reaction scope. *ACS Catal.* **8**, 701–713 (2018).
14. Perry, I. B. et al. Direct arylation of strong aliphatic C–H bonds. *Nature* **560**, 70–75 (2018).
15. Shen, Y., Gu, Y. & Martin, R. sp^3 C–H arylation and alkylation enabled by the synergy of triplet excited ketones and nickel catalysts. *J. Am. Chem. Soc.* **140**, 12200–12209 (2018).
16. Cao, H. et al. Photoinduced site-selective alkenylation of alkanes and aldehydes with aryl alkenes. *Nat. Commun.* **11**, 1956 (2020).
17. Laudadio, G. et al. C(sp^3)–H functionalizations of light hydrocarbons using decatungstate photocatalysis in flow. *Science* **369**, 92–96 (2020).
18. Wan, T. et al. Accelerated and scalable C(sp^3)–H amination via decatungstate photocatalysis using a flow photoreactor equipped with high-intensity LEDs. *ACS Cent. Sci.* **8**, 51–56 (2021).
19. Schultz, D. M. et al. Oxyfunctionalization of the remote C–H bonds of aliphatic amines by decatungstate photocatalysis. *Angew. Chem. Int. Ed.* **56**, 15274–15278 (2017).
20. Halperin, S. D., Fan, H., Chang, S., Martin, R. E. & Britton, R. A convenient photocatalytic fluorination of unactivated C–H bonds. *Angew. Chem. Int. Ed.* **53**, 4690–4693 (2014).
21. Sarver, P. J., Bissonnette, N. B. & MacMillan, D. W. Decatungstate-catalyzed C(sp^3)–H sulfinylation: rapid access to diverse organosulfur functionality. *J. Am. Chem. Soc.* **143**, 9737–9743 (2021).
22. Capaldo, L., Quadri, L. L. & Ravelli, D. Photocatalytic hydrogen atom transfer: the philosopher's stone for late-stage functionalization? *Green Chem.* **22**, 3376–3396 (2020).
23. Guillemard, L., Kaplaneris, N., Ackermann, L. & Johansson, M. J. Late-stage C–H functionalization offers new opportunities in drug discovery. *Nat. Rev. Chem.* **5**, 522–545 (2021).
24. Yuan, Z. et al. Electrostatic effects accelerate decatungstate-catalyzed C–H fluorination using [^{18}F]- and [^{19}F]NFSI in small molecules and peptide mimics. *ACS Cat.* **9**, 8276–8284 (2019).
25. Gunay, A. & Theopold, K. H. C–H bond activations by metal oxo compounds. *Chem. Rev.* **110**, 1060–1081 (2010).
26. Nam, W., Lee, Y. M. & Fukuzumi, S. Hydrogen atom transfer reactions of mononuclear nonheme metal–oxygen intermediates. *Acc. Chem. Res.* **51**, 2014–2022 (2018).
27. Sacramento, J. J. D. & Goldberg, D. P. Factors affecting hydrogen atom transfer reactivity of metal–oxo porphyrinoid complexes. *Acc. Chem. Res.* **51**, 2641–2652 (2018).
28. Chen, J. et al. Tuning the reactivity of mononuclear nonheme manganese (IV)–oxo complexes by triflic acid. *Chem. Sci.* **6**, 3624–3632 (2015).
29. Jung, J., Kim, S., Lee, Y. M., Nam, W. & Fukuzumi, S. Switchover of the mechanism between electron transfer and hydrogen-atom transfer for a protonated manganese(IV)–oxo complex by changing only the reaction temperature. *Angew. Chem. Int. Ed.* **55**, 7450–7454 (2016).
30. Fan, X.-Z. et al. Eosin Y as a direct hydrogen-atom transfer photocatalyst for the functionalization of C–H bonds. *Angew. Chem. Int. Ed.* **57**, 8514–8518 (2018).
31. Kuang, Y. et al. Asymmetric synthesis of 1,4-dicarbonyl compounds from aldehydes by hydrogen atom transfer photocatalysis and chiral Lewis acid catalysis. *Angew. Chem. Int. Ed.* **58**, 16859–16863 (2019).
32. Yan, J. et al. A radical smiles rearrangement promoted by neutral eosin Y as a direct hydrogen atom transfer photocatalyst. *J. Am. Chem. Soc.* **142**, 11357–11362 (2020).
33. Shambayati, S. & Schreiber, S. L. in *Comprehensive Organic Synthesis* Vol. 1 (ed. Trost, B. M.) Ch. 1.10 (Pergamon, 1991).
34. Arnett, E. M., Quirk, R. P. & Burke, J. J. Weak bases in strong acids. III. Heats of ionization of amines in fluorosulfuric and sulfuric acids. New general basicity scale. *J. Am. Chem. Soc.* **92**, 1260–1266 (1970).
35. Arnett, E. M. & Wu, C. Y. Stereoelectronic effects on organic bases. III. The basicities of some saturated ethers in aqueous sulfuric acid. *J. Am. Chem. Soc.* **82**, 4999–5000 (1960).
36. Vanzin, D. et al. Experimental and computational studies of protolytic and tautomeric equilibria of erythrosin B and eosin Y in water/DMSO. *RSC Adv.* **6**, 110312–110328 (2016).
37. Mchedlov-Petrosyan, N. O., Kukhtik, V. I. & Egorova, S. I. Protolytic equilibria of fluorescein halo derivatives in aqueous-organic systems. *Russ. J. Gen. Chem.* **76**, 1607–1617 (2006).
38. Mchedlov-Petrossyan, N. O. Fluorescein dyes in solutions: well studied systems? *Kharkov Natl Univ. Bull. Chem. Ser.* **626**, 221–312 (2004).
39. Fan, X. et al. Neutral-eosin-Y-photocatalyzed silane chlorination using dichloromethane. *Angew. Chem. Int. Ed.* **58**, 12580–12584 (2019).
40. Y. R. Luo, *Comprehensive Handbook of Chemical Bond Energies* (CRC Press, 2007).
41. Cismesia, M. A. & Yoon, T. P. Characterizing chain processes in visible light photoredox catalysis. *Chem. Sci.* **6**, 5426–5434 (2015).
42. Simmons, E. M. & Hartwig, J. F. On the interpretation of deuterium kinetic isotope effects in C–H bond functionalizations by transition-metal complexes. *Angew. Chem. Int. Ed.* **51**, 3066–3072 (2012).
43. Lee, W., Jung, S., Kim, M. & Hong, S. Site-selective direct C–H pyridylation of unactivated alkanes by triplet excited anthraquinone. *J. Am. Chem. Soc.* **143**, 3003–3012 (2021).
44. Li, G. X., Hu, X., He, G. & Chen, G. Photoredox-mediated Minisci-type alkylation of N-heteroarenes with alkanes with high methylene selectivity. *ACS Catal.* **8**, 11847–11853 (2018).
45. Pitre, S. P., Muuronen, M., Fishman, D. A. & Overman, L. E. Tertiary alcohols as radical precursors for the introduction of tertiary substituents into heteroarenes. *ACS Catal.* **9**, 3413–3418 (2019).
46. Tabushi, I., Hamuro, J. & Oda, R. Free-radical substitution on adamantane. *J. Am. Chem. Soc.* **89**, 7127–7129 (1967).
47. Tabushi, I., Aoyama, Y., Kojo, S., Hamuro, J. & Yoshida, Z. Free-radical halogenation of adamantane. Selectivity and relative lifetime of 1-and 2-adamantyl radicals. *J. Am. Chem. Soc.* **94**, 1177–1183 (1972).
48. Hagmann, W. K. The many roles for fluorine in medicinal chemistry. *J. Med. Chem.* **51**, 4359–4369 (2008).
49. Nodwell, M. B. et al. ^{18}F-Fluorination of unactivated C–H bonds in branched aliphatic amino acids: direct synthesis of oncological positron emission tomography imaging agents. *J. Am. Chem. Soc.* **139**, 3595–3598 (2017).
50. Takahira, Y. et al. Electrochemical C(sp^3)–H fluorination. *Synlett* **30**, 1178–1182 (2019).
51. Gómez, L. et al. Stereospecific C–H oxidation with H_2O_2 catalyzed by a chemically robust site-isolated iron catalyst. *Angew. Chem. Int. Ed.* **48**, 5720–5723 (2009).
52. Renneke, R. F., Kadkhodayan, M., Pasquali, M. & Hill, C. L. Roles of surface protonation on the photodynamic, catalytic, and other properties of polyoxometalates probed by the photochemical functionalization of alkanes. Implications for irradiated semiconductor metal oxides. *J. Am. Chem. Soc.* **113**, 8357–8367 (1991).

Acknowledgements

We are grateful for the financial support provided by Pfizer (A-0004153-00-00, J.W.), the Ministry of Education (MOE) of Singapore (MOET2EP10120-0014 for J.W. and MOE-MOET2EP10120-0007 for X.L.), NUS (Suzhou) Research Institute, National Natural Science Foundation of China (21871205, 22071170, J.W.; 21702182, 21873081 and 22122109, X.H.), the Fundamental Research Funds for the Central Universities (2020XZZX002-02, X.H.), the State Key Laboratory of Clean Energy Utilization (ZJUCEU2020007, X.H.), the Starry Night Science Fund of Zhejiang University Shanghai Institute for Advanced Study (SN-ZJU-SIAS-006, X.H.), Beijing National Laboratory for Molecular Sciences (BNLMS202102, X. H.), CAS Youth Interdisciplinary Team (JCTD-2021-11, X.H.) and the Center of Chemistry for Frontier Technologies and Key Laboratory of Precise Synthesis of Functional Molecules of Zhejiang Province (PSFM 2021-01, X.H.). Calculations were performed on the high-performance computing system at the Department of Chemistry, Zhejiang University. The authors thank P. O'Neill and S. R. Dubbaka (Pfizer) for helpful discussions.

Author contributions

H.C. discovered and developed the reaction. H.C., J.L.P., Z.P., X.H. and J.W. conceived and designed the investigations. H.C., D.K., T.L. and L.G. performed the experiments. L.-C.Y. conducted DFT calculations. S.C. and X.L. performed the flash photolysis experiments. H.C. and J.W. wrote the manuscript.

Competing interests

The authors declare no competing interests.

Additional information

Supplementary information The online version contains supplementary material available at https://doi.org/10.1038/s44160-022-00125-1.

Correspondence and requests for materials should be addressed to Xin Hong or Jie Wu.

Peer review information *Nature Synthesis* thanks the anonymous reviewers for their contribution to the peer review of this work.

Reprints and permissions information is available at www.nature.com/reprints.

Publisher's note Springer Nature remains neutral with regard to jurisdictional claims in published maps and institutional affiliations.